Supplemental Material

Towards the Rational Design of Stable Electrocatalysts for Green Hydrogen Production

Xiangxi Wang [1,2], Shengjie Bi [1], Junming Zhang [1] and Huabing Tao [1,3,*]

[1] Stat Key Laboratory for Physical Chemistry of Solid Surfaces, Collaborative Innovation Center of Chemistry for Energy Materials and National & Local Joint Engineering Research Center for Preparation Technology of Nanomaterials, College of Chemistry and Chemical Engineering, Xiamen University, Xiamen 361005, China; wangxiven@hotmail.com (X.W.); 20620191151298@stu.xm.edu.cn (S.B.); junming001@e.ntu.edu.sg (J.Z.)

[2] National Key Laboratory of Science and Technology on Vessel Integrated Power System, Naval University of Engineering, Wuhan 430033, China

[3] Innovation Laboratory for Sciences and Technologies of Energy Materials of Fujian Province (IKKEM), Xiamen 361005, China

* Correspondence: hbtao@xmu.edu.cn

Abstract: Now, it is time to set up reliable water electrolysis stacks with active and robust electrocatalysts to produce green hydrogen. Compared with catalytic kinetics, much less attention has been paid to catalyst stability, and the weak understanding of the catalyst deactivation mechanism restricts the design of robust electrocatalysts. Herein, we discuss the issues of catalysts' stability evaluation and characterization, and the degradation mechanism. The systematic understanding of the degradation mechanism would help us to formulate principles for the design of stable catalysts. Particularly, we found that the dissolution rate for different 3d transition metals differed greatly: Fe dissolves 114 and 84 times faster than Co and Ni. Based on this trend, we designed Fe@Ni and FeNi@Ni core-shell structures to achieve excellent stability in a 1 A cm^{-2} current density, as well as good catalytic activity at the same time.

Keywords: core-shell; stability; water splitting; hydrogen production; oxygen production

1. Experimental Detail

1.1. Materials and Reagents

To reduce the effects of impurities, high purity KOH (semiconductor grade, 99.99% trace metals basis, Sigma-Aldrich) was used as the alkaline electrolyte. The potential of SCE in 1 M KOH electrolyte was calibrated to be 1.049 V vs. RHE. Pure 3d transition metals were purchased from Hebei Qinghe Changsheng metal Co., LTD with purity above 99.99%.

1.2. Materials Synthesis

The core-shell Fe@Ni nanoparticles were synthesized as: 1 mmol of iron (III) chloride hexahydrate, 1 mmol of nickel (II) chloride hexahydrate, and 4 mmol of sodium borohydride were separately added into 20 mL deionized (DI) water. The sodium borohydride solution was then sonicated under N$_2$ atmosphere to maintain an oxygen free environment. Subsequently, iron chloride solution was added dropwisely to the sonicated sodium borohydride solution to prepare small Fe nanoparticles. After 30 min of ultrasonication, nickel chloride solution was added and stirred for another 10 min to obtain coreshell Fe@Ni nanoparticles.

The homogeneous FeNi catalyst was prepared by a simple electrochemical deposition method. Fluorine-doped SnO$_2$ (FTO) glass, carbon electrode, and a saturated calomel electrode (SCE) worked as the working, counter, and reference electrode, respectively.

The electrolyte was obtained by mixing 0.1 M $FeSO_4$ and 0.1 M $Ni(NO_3)_2$ aqueous solution. The applied potential was −1.0 V vs. SCE, and the electrodeposition time was 90 s.

1.3. Electrochemical Studies

Electrochemical tests were conducted on a CHI 760e workstation (CH Instruments Ins) with a three-electrode configuration. Specially designed glass-free cell (provided by Hangzhou Saiao Electrochemical Technology Co., LTD) was used in alkaline OER tests to eliminate the influence of glass components on the activity of catalysts.[32] Pt plate (1 cm^2) was used as the counter electrode only in the OER tests. SCE was used as the reference electrode. Working electrodes were pure metals with active area of 1 cm^2. Characterizations of catalyst dissolution were conducted in the chronoamperometric mode for 12 hours with current density of 50 mA/cm^2. Electrolyte after stability test was monitored by ICP-MS to determine the dissolved concentration of metal elements.

1.4. UV-vis Spectroscopy Study of Dissolved FeO_4^-

To identify the dissolution pathway of Fe, we employed UV-vis spectroscopy to detect FeO_4^{2-}, which has a maximum absorption around 510 nm. [33] From the start of the stability test of Fe electrode in OER, the color of electrolyte changed to pale violet (the typical color of FeO_4^{2-}) within minutes, indicating the generation of FeO_4^{2-}. However, the yellow precipitate formed subsequently, which should be originated from the decomposition of FeO_4^{2-}. The observation is consistent with the UV-vis spectroscopy result obtained during the stability test as shown in Fig. S2.

1.5. Inductively Coupled Plasma-Mass Spectrometry (ICP-MS) Study

The ICP-MS study was used to measure the dissolution rate of samples. After 24 h of stability test, the 30 mL electrolyte (1 M KOH) was dissolved with 10 mL 3.5 M HCl solution, then 2 mL of the solution was mixed with 8 mL DI water to obtain 10 mL solution A. The counter electrode was also washed with 10 mL 1.0 M HCl solution and followed the same step to obtain 10 mL solution B. Afterwards, the two solutions were tested by ICP-MS.

1.6. X-ray Photoelectron Spectroscopy (XPS) Etching Procedure

The XPS etching procedure was used to identify the ratio of Fe and Ni element in different depth. Etching speed Ta_2O_5 = 0.16 nm/s, etching time 18 s every step. In this conditions, the etching depth is Ta_2O_5 =2.88 nm every step.
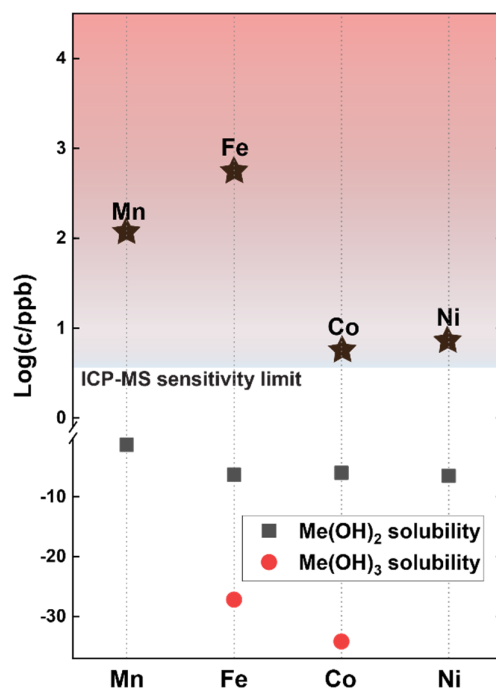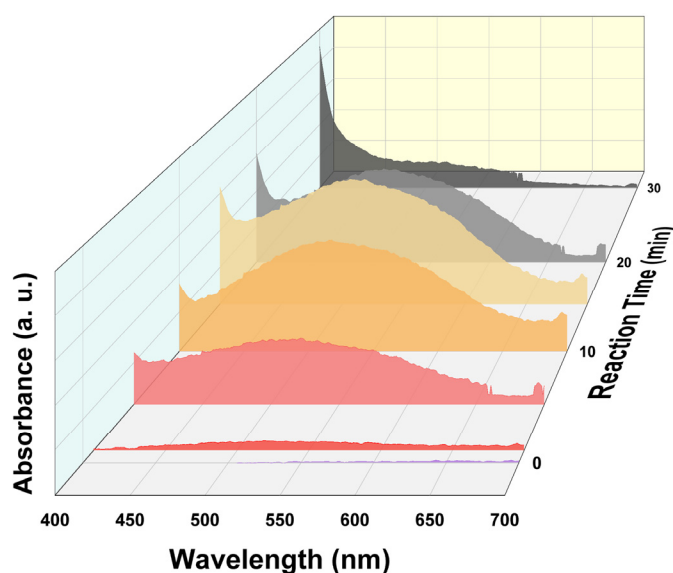
2. Supporting Data and Discussion

Table S1. Calculated solubility of hydroxide for various 3d transition metals.

Metal hydroxide	K_{sp}	Solubility (mol/L)	Solubility (ppb wt.)	log(solubility/ppb)
$Mn(OH)_2$	9.0×10^{-11}	9.0×10^{-11}	5.0×10^{-2}	−1.3
$Fe(OH)_2$	1.0×10^{-15}	1.0×10^{-15}	5.6×10^{-7}	−6.3
$Fe(OH)_3$	1.1×10^{-36}	1.1×10^{-36}	6.2×10^{-28}	−27.2
$Co(OH)_2$	1.6×10^{-15}	1.6×10^{-51}	9.4×10^{-7}	−6.0
$Co(OH)_3$	1.0×10^{-43}	1.0×10^{-43}	5.9×10^{-35}	−34.2
$Ni(OH)_2$	5.5×10^{-16}	5.5×10^{-16}	3.2×10^{-7}	−6.5
$Cr(OH)_2$	2.0×10^{-16}	2.0×10^{-16}	1.0×10^{-7}	−7.0
$Cr(OH)_3$	6.3×10^{-31}	6.3×10^{-31}	3.3×10^{-22}	−21.5

Note: Solubility product constant (K_{sp}) was derived from ref. [34] The solubility of all the hydroxides listed in the table is orders of magnitude lower than the detection limit of state-of-the-art instrument (ICP-MS), where only above 1 ppb can be detected. Therefore, the dissolved components should not be the hydroxides.

Table S2. ICP-MS results of the dissolved 3d transition metals.

Element	Dissolved quantity (ppb wt.)	Dissolution rate ($\mu g\ h^{-1} cm^{-2}$)
Mn	148.8	2.9
Fe	603.5	50.3
Co	5.3	0.44
Ni	7.2	0.6

Figure S1. Comparison between ICP-MS results with the solubility of metal hydroxides. The solubility of the metal hydroxides are orders of magnitude lower than the sensitivity of ICP-MS, implying that the dissolved metals should not be in the form of metal hydroxides.

Figure S2. Detection of FeO_4^{2-} evolved from Fe electrode in OER by UV-vis spectroscopy. The maximum absorption occurs around 510 nm. The absorption increases from the start of reaction, and then decreases over time.
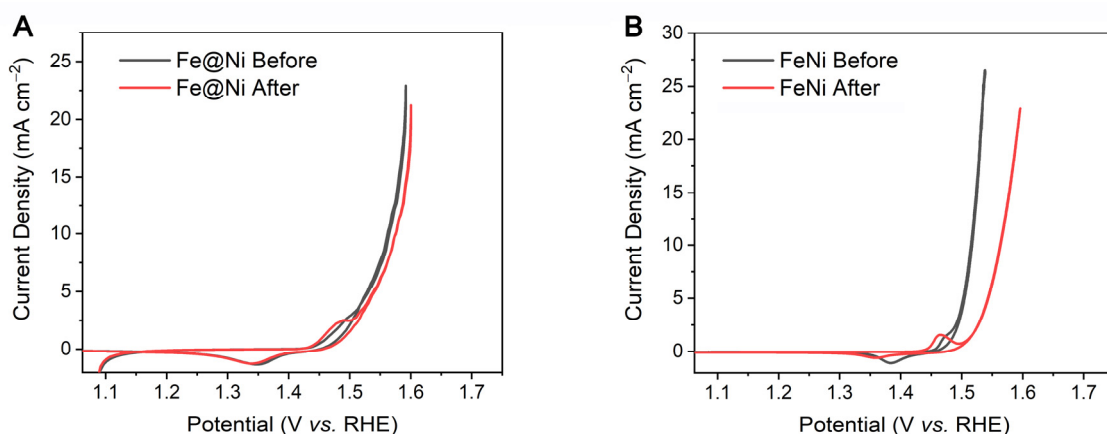
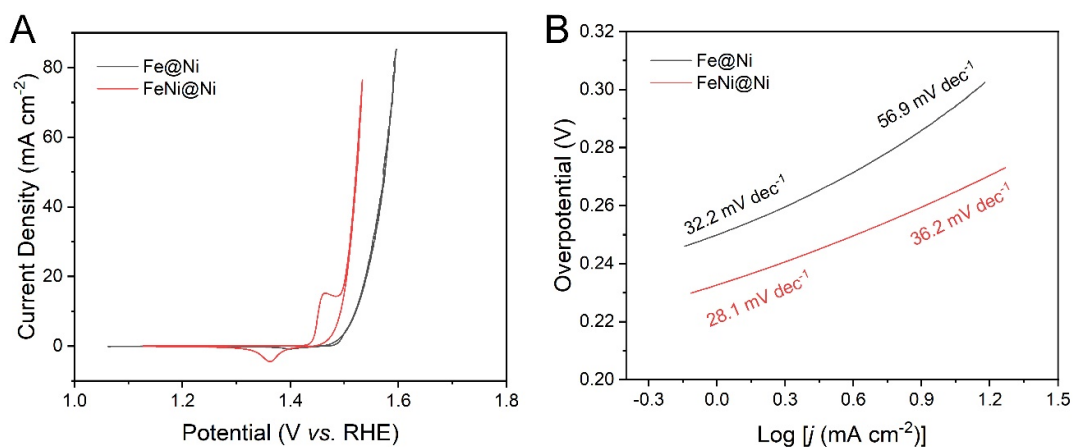**Figure S3.** LSV curves before and after 24 h chronopotentiometry test of Fe@Ni (**A**) and FeNi (**B**).

Figure S4. LSV curves of Fe@Ni and FeNi@Ni (**A**) and corresponding Tafel slope (**B**).
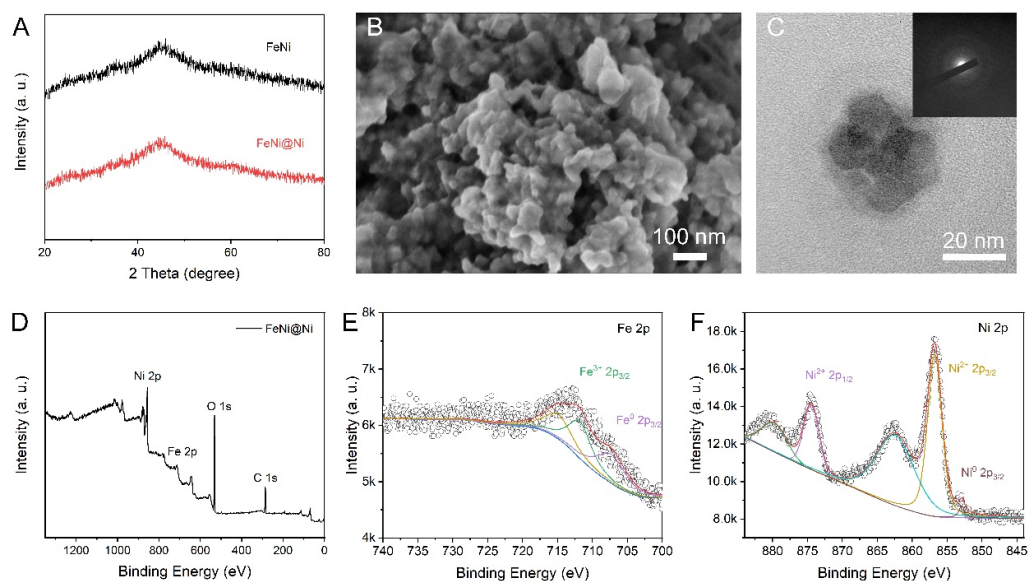

Figure S5. X-ray diffraction pattern for FeNi and FeNi@Ni (**A**). The SEM image for FeNi@Ni catalysts (**B**). The TEM and SAED image (**C**). Corresponding XPS and high-resolution Fe 2p and Ni 2p XPS patterns (**D–F**).
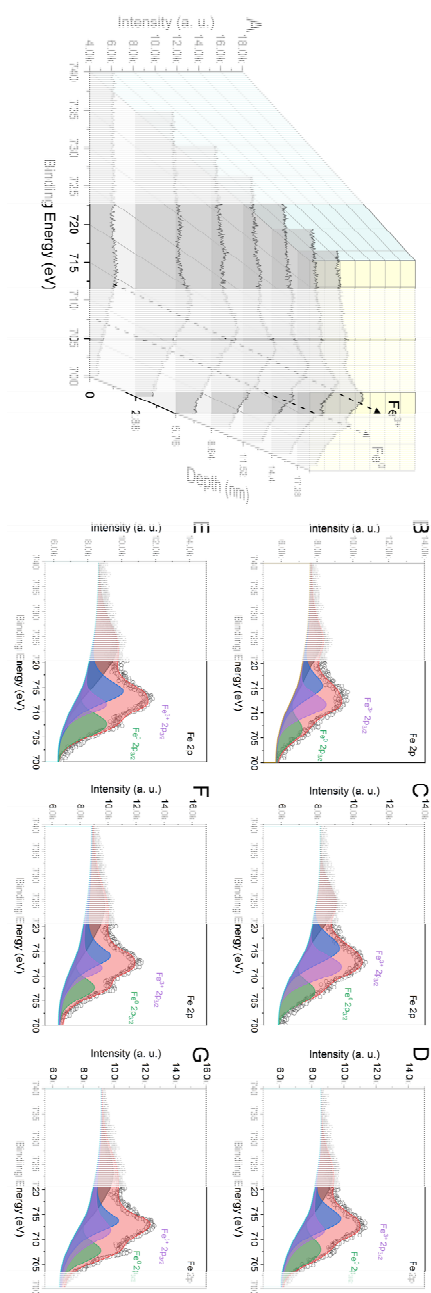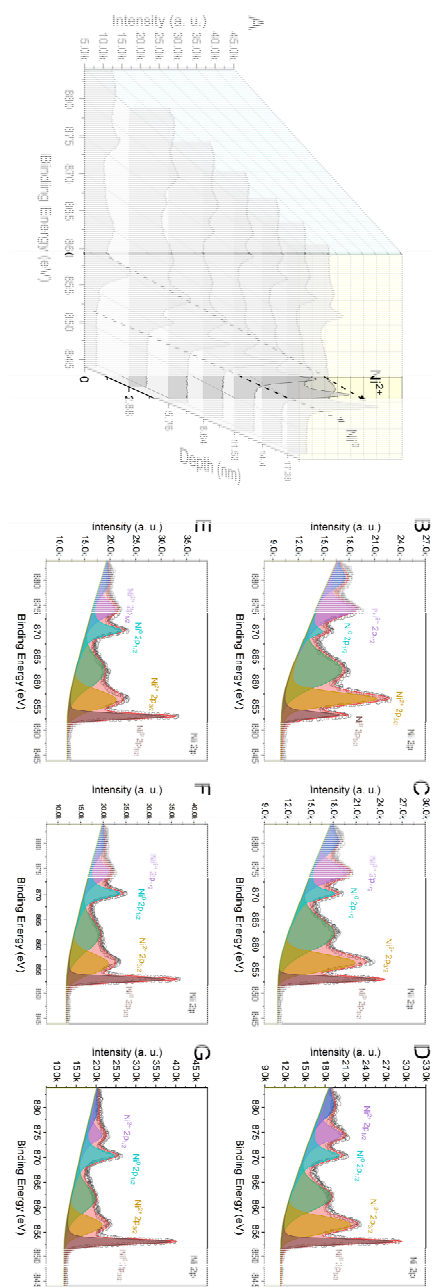
Figure S6. XPS etching test for FeNi@Ni catalysts. The comparison of high-resolution Fe 2p XPS curves in different etching step (**A**), 2.88 nm etching (**B**), 5.76 nm etching (**C**), 8.64 nm etching (**D**), 11.52 nm etching (**E**), 14.40 nm etching (**F**), 17.28 nm etching (**G**).

Figure S7. XPS etching test for FeNi@Ni catalysts. The comparison of high-resolution Ni 2p XPS curves in different etching step (**A**), 2.88 nm etching (**B**), 5.76 nm etching (**C**), 8.64 nm etching (**D**), 11.52 nm etching (**E**), 14.40 nm etching (**F**), 17.28 nm etching (**G**).
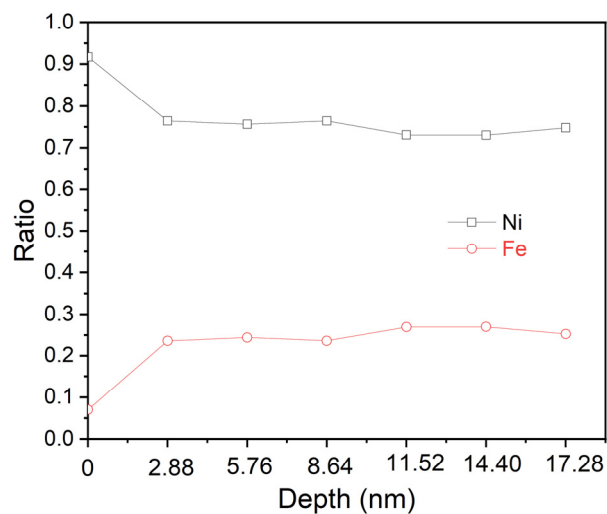
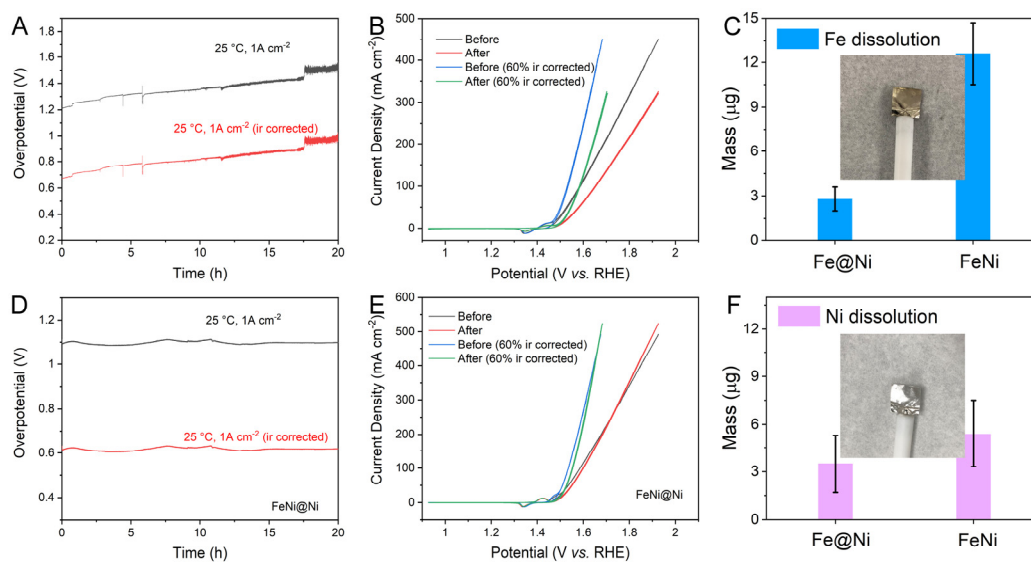**Figure S8.** The contrast of Ni and Fe content in FeNi@Ni structure with different depth.

Figure S9. The chronopotentiometry test at current density of 1 A cm^{-2} for FeNi (**A**) and FeNi@Ni (**D**), the corresponding before and after CV curves (**B**,**E**), the ICP test for Fe and Ni dissolution (**C**,**F**).
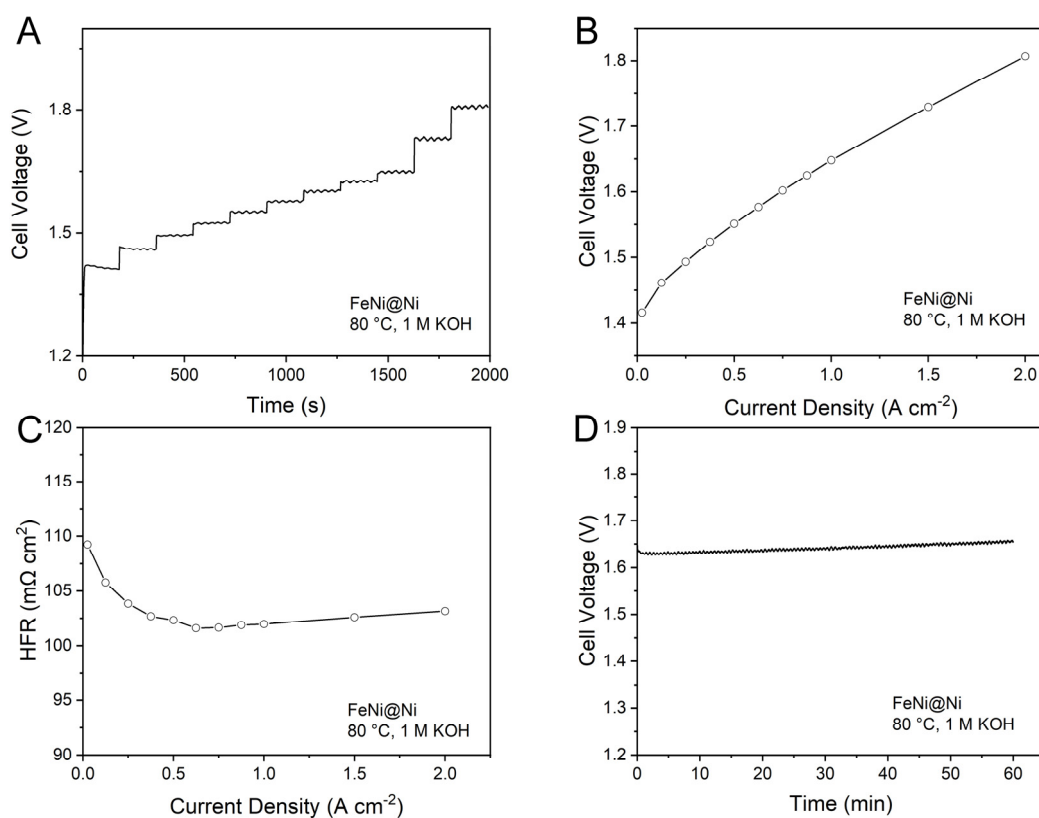
Figure S10. AEMWEs performance at 80 °C and 4M KOH. (**A,B**) Polarization curve of AEMWE single cell with FeNi@Ni anode coupled with commercial Pt/C (60%) cathode. (**C**) The HFR pattern for single cell. (**D**) Stability test for single cell at cell voltage of 1 A cm$^{-2.}$